Inverse scattering approach to multiwavelength Fabry-Pérot laser design

S. O'Brien,[1] S. Osborne,[1] K. Buckley,[1] R. Fehse,[1] A. Amann,[1] E. P. O'Reilly,[1] L. P. Barry,[2] P. Anandarajah,[2] J. Patchell,[3]
and J. O'Gorman[3]

[1]*Tyndall National Institute, University College, Lee Maltings, Cork, Ireland*
[2]*RINCE, School of Electronic Engineering, Dublin City University, Dublin 9, Ireland*
[3]*Eblana Photonics, Trinity College Enterprise Centre, Pearse Street, Dublin 2, Ireland*

A class of multiwavelength Fabry-Pérot lasers is introduced where the spectrum is tailored through a patterning of the cavity effective index. The cavity geometry is obtained using an inverse scattering approach and can be designed such that the spacing of discrete Fabry-Pérot lasing modes is limited only by the bandwidth of the inverted gain medium. A specific two-color semiconductor laser with a mode spacing in the THz region is designed, and measurements are presented demonstrating the simultaneous oscillation of the two wavelengths. The nonperiodic effective index profile of the particular two-color device considered is shown to be related to a Moiré or superstructure grating.

( )

The most familiar laser cavity geometry is the Fabry-Pérot (FP) laser, which comprises an active gain medium and two external mirrors providing feedback for oscillation. In this geometry the longitudinal lasing mode wavelengths are determined by the half-wave resonance condition: $\lambda^m = 2nL_c/m$, where $m = 1, 2, \ldots$, λ^m is the free space wavelength of the mth mode, L_c is the cavity length, and n is the cavity refractive index [1].

A fundamental limitation of the basic FP geometry is the lack of any frequency selectivity other than that provided by the gain medium. Because the gain bandwidth is much larger than the FP mode spacing in typical semiconductor lasers, more complex laser cavity geometries have been conceived in order to control and manipulate semiconductor laser spectra. For example, one dimensional systems such as the distributed feedback laser (DFB) provide high spectral purity and temperature stability in device applications [2]. Translational symmetry determines the lasing modes of this structure without the need for a reflection from external mirrors. Approaches to designing multiwavelength devices have also been proposed, including DFB lasers with many spatial frequencies present in the grating [3], and dual mode distributed Bragg reflector lasers, which incorporate tunable mirror sections [4].

If we consider the interaction of the cavity modes with the gain medium, the semiconductor FP laser geometry is deceptively simple. In a perfectly homogeneously broadened medium, a single lasing mode should always dominate [5,6]. When driven above threshold, semiconductor FP lasers often oscillate in many modes. This multimode behavior is characteristic of inhomogeneously broadened gain media, despite the fact that in a semiconductor the carriers are distributed in continuous bands.

A key property of the FP laser in this respect is the fact that all the cavity resonant wave vectors are equally spaced. As a result, four-wave mixing (FWM) interactions, which transfer power among modes, are cavity enhanced. In addition, carrier density pulsations at the intermode frequencies and the finite linewidth enhancement or alpha factor lead to an asymmetric contribution to the nonlinear gain in semiconductor lasers [7–9]. This interaction also promotes multi-

mode oscillation and can lead to mode hopping and complex antiphased switching dynamics [10,11].

In this paper we revisit and extend the basic FP laser geometry. We demonstrate that multiwavelength FP lasers can be designed where, apart from the constraint imposed by the half-wave resonance requirement, the distribution of lasing modes is chosen *independent* of the cavity length. The basic FP cavity configuration and mode structure are maintained, with the manipulation of the lasing mode spectrum achieved using a nonperiodic effective index profile. The precise geometry is determined from the desired lasing spectrum through an inverse scattering approach [12,13].

Because of its fundamental significance, we present experimental measurements of a two-color semiconductor FP laser with a primary mode spacing in the THz regime. Our measurements demonstrate that the device oscillates simultaneously on two discrete FP modes, and without the requirement for an external cavity arrangement or other external perturbation. In contrast to this ideal behavior associated with weakly coupled modes, an otherwise identical *plain* FP laser, with a modal spacing determined by the cavity length, displays the mode hopping behavior and complex dynamics associated with strong mode competition.

Consider the one-dimensional model of the FP cavity geometry represented in Fig. 1. The system comprises a FP cavity of length L_c with a spatially varying refractive index. The mirror reflectivities are r_1 and r_2 (assumed real for simplicity) and there are N additional index steps along the cavity. For each section of the laser cavity (index i) we define $\theta_i = n_i k_{0z} L_i$, where k_{0z} is the free space wave number along z and L_i and n_i are the length and the effective refractive index of the ith section, respectively. The adjusted complex optical path length across the cavity is then $\Sigma_{i=1}^{2N+1} \theta_i$.

We set the background cavity effective index, $n_1 = n$, and the effective index at the index step features, $n_2 = n + \Delta n$. Suppose the transfer matrix T relates the right and left moving electric fields, $E^\pm(z)$, at the cavity mirrors in Fig. 1. Then the lasing modes of the cavity are defined by the relation [13]
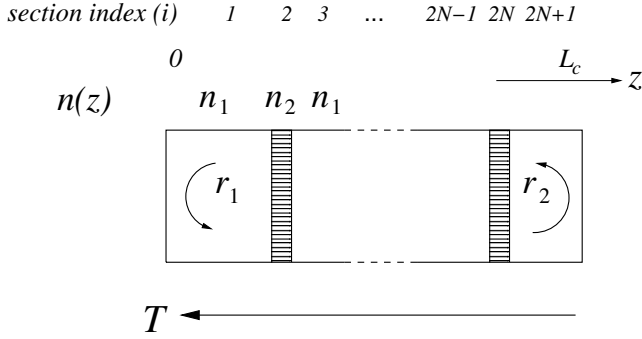
FIG. 1. One dimensional model of a Fabry-Pérot laser cavity of length L_c and including N index steps. The cavity effective index is n_1 while the additional features providing the index step (shaded regions) have effective index n_2 as shown. All cavity sections are numbered $1 \leq i \leq 2N+1$ beginning on the left. The matrix T relates the left and right moving fields inside the cavity at the cavity mirrors. The mirror reflectivities are r_1 and r_2 as shown.

$$T_{11} - T_{22}r_1r_2 = T_{21}r_1 - T_{12}r_2. \tag{1}$$

From Eq. (1) one can show that the lasing condition at first order in the index step can be written

$$1 - r_1r_2 \exp(2i\Sigma\,\theta_i) = i\frac{\Delta n}{n}\sum_j\, \sin\,\theta_{2j}[r_1 \exp(2i\phi_j^-)$$
$$+ r_2 \exp(2i\phi_j^+)], \tag{2}$$

where the quantities ϕ_j^- and ϕ_j^+ are the optical path lengths from the center of each additional feature to the left and right facets, respectively. In deriving Eq. (2) we have made a first-order Born approximation when calculating the transfer matrix T. In this way we neglect multiple scattering between (and within) the additional features. It should be noted, however, that this expression for the lasing threshold condition describes the coupling between each feature and the external mirrors exactly.

If we neglect a factor describing the background losses associated with each mode, for a vanishing index step, the threshold gain for lasing is determined by the mirror losses. We have $\gamma_m^{(0)} = L_c^{-1} \ln 1/r_1r_2$. In the perturbed case, a set of self-consistent equations for the lasing modes is found by making an expansion in Eq. (2) about the cavity resonance condition: $\Sigma\,\theta_i' = \phi_j^{-'} + \phi_j^{+'} = m\pi + \delta_m$ [13], where $\delta_m(\ll 1)$ determines the lasing mode frequency shift.

The inverse problem at first order is solved by choosing a particular cavity resonance, m_0, as an origin in wave number space. We assume quarter wave features with $\sin\,\theta_{2j}' = 1$ in order that the intensity scattered by each feature at the wavelength of mode m_0 is maximized. Taking the limit of a vanishing index step Δn, we at first neglect the optical path length corrections which result from the introduction of the additional features. In this limit distances along the cavity are proportional to the corresponding change in the optical path. One finds that the effect of the spatially varying refractive index is maximized where each feature is placed such that a half wavelength subcavity at the wavelength of mode m_0 is formed between the feature and one of the external
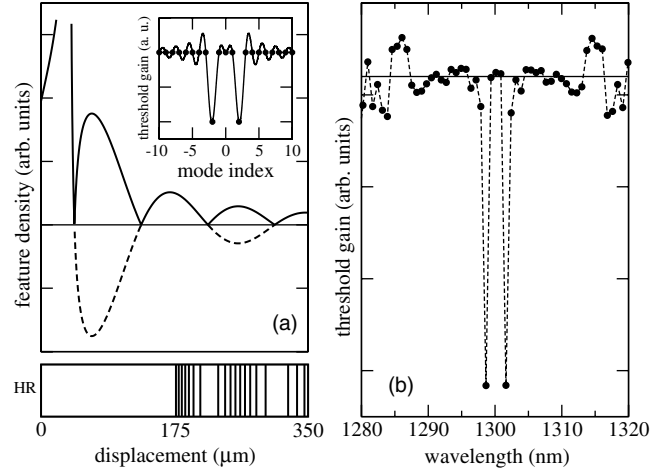

FIG. 2. (a) Feature density function (solid line). The dashed lines are the negative of the feature density function in those intervals where the Fourier transform of the function shown in the inset is negative. Inset: Ideal threshold gain of modes in wave number space. Lower panel: Laser cavity schematic indicating the locations of the additional features. The device is high-reflection coated as indicated. (b) Calculation of the threshold gain of modes for the laser cavity schematically pictured in the lower panel of the figure. The horizontal line is at the value of the mirror losses of the plain cavity.

mirrors. The threshold gain can then be expressed at each resonance, m, where $m = m_0 + \Delta m$, as $\gamma_m = \gamma_m^{(0)} + (\Delta n/n)\gamma_m^{(1)}$, where

$$\gamma_m^{(1)} = \frac{1}{L_c\sqrt{r_1r_2}} \cos(m_0\pi)\cos(\Delta m\pi)$$
$$\times \sum_{j=1}^{N} A(\epsilon_j)\sin(2\pi\epsilon_j m_0)\cos(2\pi\epsilon_j\Delta m). \tag{3}$$

In the above expression, the factor $A(\epsilon_j) = r_1 \exp(\epsilon_j L_c \gamma_m^{(0)}) - r_2 \exp(-\epsilon_j L_c \gamma_m^{(0)})$ and ϵ_j is the position of the center of each feature measured from the center of the cavity as a fraction of the cavity length.

Using Eq. (3) Fourier analysis can be used in order to build up a particular threshold gain spectrum in wave number space. Because it represents the simplest system that illustrates the application of classical multimode laser theory [14], the multiwavelength device we describe here is the two-color laser. The appropriate basis for this device is a pair of sinc functions, $\gamma_m^{(1)} \sim \mathrm{sinc}(\Delta m + a/2) + \mathrm{sinc}(\Delta m - a/2)$. This choice selects two modes, centered at m_0 and with spacing a modes, while leaving the other FP modes unperturbed. In the inset of Fig. 2(a) we have plotted an idealized threshold gain spectrum where the primary mode spacing is $a = 4$ fundamental cavity modes. The Fourier transform of our idealized threshold modulation function is $\cos(\pi a\epsilon)$, for $-1/2 \leq \epsilon \leq 1/2$ and is zero otherwise.

The change in threshold of a given mode is determined by the difference in the roundtrip amplitude gain to the left and to the right of each feature. To determine the appropriate distribution of features, we must therefore correct for the

variation of the amplitude of the threshold modulation with position. We take the product of the Fourier transform of our ideal threshold modulation function with the envelope function, $[A(\epsilon_j)]^{-1}$. The absolute value of this product determines the feature density function shown in Fig. 2(a), which is sampled over the appropriate interval in order to approximately reproduce the idealized threshold gain spectrum. The approximate feature positions are given by the solutions of the following equation:

$$C \int^{\epsilon_j} [A(x)]^{-1} |\cos(\pi a x)| dx = j - 1/2. \qquad (4)$$

Here C is normalized to the number of features to be introduced, and $j = 1, 2, \ldots, N$.

For the two-color device considered the cavity is asymmetric with one larger facet reflectivity (r_1). This allows a more uniform density of features along one side of the device center. Once the feature density function is sampled correctly, feature positions are adjusted in order to satisfy the correct phase requirement for resonance. A schematic picture of the device, high-reflection coated as indicated, is shown in the lower panel of Fig. 2. With respect to the lasing wavelength of mode m_0 in the cavity, where $\cos(\pi a \epsilon_j) > 0$, the phase requirement corresponds to forming a half-wave resonant subcavity between the corresponding feature and the high-reflection coated mirror. For $\cos(\pi a \epsilon_j) < 0$, we form a quarterwave subcavity at the same wavelength. In this way, at each zero of the feature density function a $\pi/2$ phase shift is introduced into the index pattern along the device length. Optical path corrections due to the introduction of the features must also be accounted for when the final feature positions are calculated [13]. The calculated form of the threshold gain spectrum is shown in Fig. 2(b) and is an excellent approximation of the ideal form. Note that the device comprises a single, patterned amplifying section with both external mirrors necessary to form the FP mode structure. Thus, unlike distributed feedback approaches, the role of the inhomogeneous cavity effective index is simply to discriminate between the various FP modes.

We note also that in the particular case of a two-color FP laser formed by a pair of sinc functions as above, the refractive index pattern is related to that of a Moiré grating. The index of refraction of a Moiré or superstructure grating is given by [15]

$$n(z) = n_0 + \Delta n \cos\left(\frac{2\pi}{\Lambda_s}\right) \cos\left(\frac{2\pi}{\Lambda}\right), \qquad (5)$$

where n_0 is the average index, Λ is the Bragg period and Λ_s is the superstructure period. Fiber Bragg gratings of the Moiré type are of considerable interest in slow-light and dispersion management systems. If we neglect the envelope function $A(\epsilon)$, sampling of the Fourier transform $\cos(\pi a \epsilon)$ and adjusting for resonance as described generates a finite section of Moiré grating where the number of superstructure periods between the cavity mirrors is equal to half the primary mode spacing. Inclusion of the envelope function then determines a "sampled" Moiré grating section, where the average density is nonuniform and an additional $\pi/2$ phase
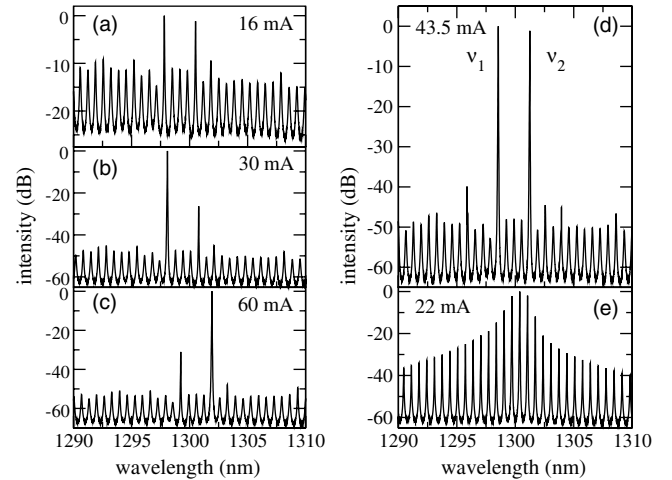

FIG. 3. (a) Below threshold spectrum of the two-color device of Fig. 2. (b) Lasing spectrum at 30 mA. (c) Lasing spectrum at 60 mA. (d) Two-color lasing spectrum at 43.5 mA. (e) Above threshold spectrum of a plain Fabry-Pérot device fabricated on the same bar.

shift is required where $A(\epsilon)$ vanishes. The region containing this point, ($\epsilon < 0$), is avoided in the asymmetric device considered here.

We now present experimental measurements of a ridge wave guide FP laser fabricated to the design depicted in Fig. 2. The device is a multiquantum well $InP/Al_xGa_yIn_{1-x-y}As$ laser of length 350 μm with a peak emission near 1.3 μm. The additional features are slotted regions etched into the laser ridge wave guide. This technique is based on standard optical lithography and does not require a regrowth step. The laser was temperature stabilized at 25 °C to ± 0.01 °C and a constant current was applied to the device. The laser emission was coupled into an optical fiber. A lens was used to collimate the laser emission and another lens was used to focus the collimated beam onto the fiber. Both lenses had anti-reflection coatings and an optical isolator was placed between the lenses to reduce the effect of external reflections. The fiber coupled laser emission was then characterized using an optical spectrum analyzer with 0.01 nm resolution and an autocorrelator.

A series of spectra of the device of Fig. 2 are shown in Fig. 3. Figure 3(a) shows the device spectrum below threshold. One can see that the two primary modes are already selected in this regime. Note the good agreement with the calculation shown in Fig. 2, with the two primary modes separated by four fundamental FP modes. The discrepancy in the primary mode wavelengths between the theoretical calculation and the experimental results can be attributed to a difference in the refractive index of the device from that anticipated and to our neglect of refractive index dispersion in Fig. 2. As the current is increased the mode on the short wavelength side reaches threshold first [Fig. 3(b)] and as the current is increased further thermal effects lead to the peak power shifting across the primary mode spacing to the long wavelength side [Fig. 3(c)]. The lasing spectrum at 43.5 mA is shown in Fig. 3(d). At this current the time averaged optical power in the primary modes is approximately equal. For
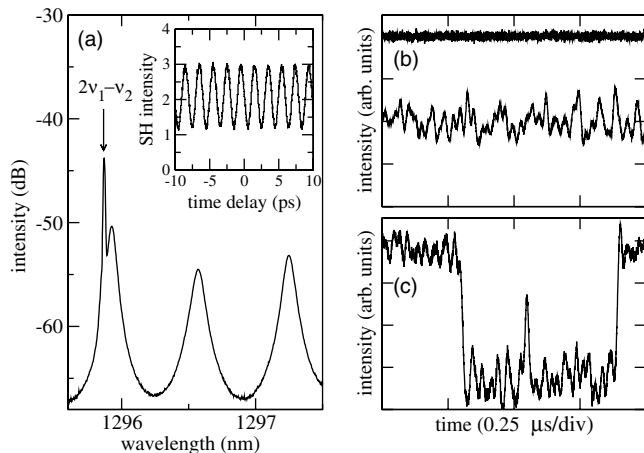
FIG. 4. (a) Enlarged spectrum showing the presence of a four-wave mixing sideband. Inset: Background free intensity autocorrelation measurement showing mode beating at 480 GHz. (b) Time traces of a primary mode (lower trace) and total device output (upper trace) showing essentially constant total output. Not shown is the second primary mode output which is anticorrelated with the first. (c) Time trace of the output of a single FP laser mode from the device of Fig. 3(e). At this current the plain FP laser is exhibiting mode-hopping behavior.

comparison, an above threshold spectrum from a plain FP laser fabricated on the same bar is shown in Fig. 3(e).

Detail from the spectrum of Fig. 3(d) is plotted in Fig. 4(a). One can see sideband formation due to four wave mixing (FWM) processes in the cavity. FWM is a third order nonlinear process which occurs due to the formation of a dynamic grating in the material complex index [16,17]. The grating is formed through the beating of the primary modes at ν_1 and ν_2 as shown in Fig. 3(d). The sideband shown appears at a frequency of $2\nu_1 - \nu_2$ with the scattering of the primary mode at ν_1 by the grating. Within the bandwidth of the inverted semiconductor, the patterned FP cavity naturally provides gain and resonant feedback for the FWM sideband, which is slightly detuned from the amplified spontaneous emission peak due to the material dispersion. The presence of a large, narrow linewidth signal, implies that the two modes are oscillating simultaneously with good phase stability.

Phase coherence of the primary modes implies an ultrafast intensity modulation of the laser output. We measured this mode beating in the cw output of the laser at the difference frequency, $\nu_2 - \nu_1 \sim 480$ GHz. The result of the background free intensity autocorrelation measurement is shown in the inset of Fig. 4(a) where the contrast ratio observed is close to the theoretical limit of 3:1, expected for two sine waves of equal amplitude. In the mode locking regime, the extension of concepts described here to create a comb of discrete wavelengths can lead to compact sources of pulsed radiation with THz repetition rates. In fact, the polarization associated with the mode beating itself is a potential source of direct THz radiation, generated in an intracavity process [18]. Such systems have received considerable interest on account of their potential to enhance nonlinear interactions. Approaches to intracavity wave mixing have tended to focus on engineering

of the semiconductor heterostructure to support distinct optical transitions and thus multiple lasing wavelengths [19,20]. The extension of the FP cavity concept described here represents a complimentary means to design such a system where the suppression of unwanted longitudinal cavity mode structure can further improve the efficiency.

We now apply the semi-classical theory of a homogeneously broadened two mode laser to our device near the current of Fig. 3(d). In semi-classical laser theory, simultaneous lasing of two modes is possible if the net gain of each mode is positive and the competition due to cross saturation is sufficiently weakened by a large mode spacing and by the spatial hole burning effect associated with the standing waves of the FP cavity [14].

Measurements of time traces of the modal and total intensity output of the two-color device are shown in Fig. 4(b). To measure the temporal evolution of the individual lasing modes the laser emission was spectrally resolved. The collimated laser beam, which had passed through an optical isolator, was incident on a grating (1200 lines/mm). The diffracted beam was spatially filtered to isolate emission from one mode. A 50:50 beam splitter was also inserted before the grating allowing measurement of the total output power. The bandwidth (50 MHz) of the system was limited by the detector used. In Fig. 4(b), we observe an essentially constant total output and anticorrelated, enhanced intensity noise traces in each of the two primary modes due to mode partition (a single modal intensity time trace is shown for clarity) [21]. As is indicated by the spectral and autocorrelation measurements, the two-color device is thus not exhibiting the mode hopping behavior characteristic of multiwavelength lasers with strongly coupled lasing modes [22]. The plain FP laser of Fig. 3(e) also shows a constant total intensity, but analysis of individual modal intensities reveals complex dynamics including mode hopping behavior, an example of which is shown in Fig. 4(c). This figure shows a sequence of spontaneous switching events where the longitudinal mode in question switches between an "on" state with large intensity to an "off" state with an intensity close to zero.

In the two-color device here, the coupling between the primary modes is determined by various processes that have different strengths depending on the separation between the modes. These include static spectral hole burning, intraband population pulsations, and carrier density pulsations. Because the characteristic time associated with interband processes is large, the contribution of asymmetric nonlinear gain due to the interband carrier density pulsations will be much smaller in the two-color device, where the separation between modes is large. If we neglect the asymmetric contribution, weak coupling of modes in the two-color device requires $(4/3) \cdot [1 + (\omega_1 - \omega_2)^2 \tau_{\text{in}}^2]^{-1} < 1$, where $\omega_{1,2} = 2\pi\nu_{1,2}$ and τ_{in} is the intraband relaxation time [9]. An estimated range of values for τ_{in} is 100–200 fs, which determines a minimum spacing for the two modes of 460–920 GHz. Although this estimate is in agreement with the actual modal separation and stability properties observed, a systematic study of two-color and other multiwavelength FP lasers will be of interest in order to understand separately the roles of the primary mode spacing and the total mode number in determining the stability and dynamical properties of this family of devices.

()

The stability property of the two-color lasing spectrum may also lead to significant applications. For example, the THz primary mode spacing of the devices makes them suitable for the optical generation of THz radiation by photomixing. Because of their stable operation, they are also potentially a simple switchable source of two widely spaced quasisingle mode wavelengths as shown in Fig. 3.

In conclusion, we have introduced a class of multiwavelength Fabry-Pérot lasers where the number and spacing of the lasing modes is limited only by the bandwidth of the active medium. Measurements of simultaneous lasing in a specially designed two-color Fabry-Pérot cavity geometry with THz mode spacing were presented. The inverse scattering approach to multiwavelength laser design described is likely to open up new avenues for the fundamental studies of semiconductor laser stability and dynamics. In addition, the devices can provide interesting solutions to many applied problems in optoelectronics and nonlinear optics.

[1] G. P. Agrawal and N. K. Dutta, *Long-Wavelength Semiconductor Lasers* (Van Nostrand Reinhold, New York, 1986).

[2] H. Kogelnik and C. V. Shank, Appl. Phys. Lett. **18**, 152 (1971).

[3] A. Talneau, J. Charil, and A. Ougazzaden, Appl. Phys. Lett. **75**, 600 (1999).

[4] S. D. Roh, T. S. Yeoh, R. B. Swint, A. E. Huber, J. S. Woo, and J. J. Coleman, IEEE Photon. Technol. Lett. **12**, 1307 (2000).

[5] H. Haken, *Laser Theory* (Springer-Verlag, Berlin, 1986).

[6] A. Tredicuicci, C. Gmachl, F. Capasso, D. L. Sivco, A. L. Hutchinson, and A. Y. Cho, Nature (London) **396**, 350 (1998).

[7] M. Yamada, J. Appl. Phys. **66**, 81 (1989).

[8] A. Uskov, J. Mork, J. Mark, M. C. Tatham, and G. Sherlock, Appl. Phys. Lett. **65**, 944 (1994).

[9] S. Ogita, A. J. Lowery, and R. S. Tucker, IEEE J. Quantum Electron. **33**, 198 (1997).

[10] M. Ahmed and M. Yamada, IEEE J. Quantum Electron. **38**, 682 (2002).

[11] A. M. Yacomotti, L. Furfaro, X. Hachair, F. Pedaci, M. Giudici, J. Tredicce, J. Javaloyes, S. Balle, E. A. Viktorov, and P. Mandel, Phys. Rev. A **69**, 053816 (2004).

[12] S. O'Brien and E. P. O'Reilly, Appl. Phys. Lett. **86**, 201101 (2005).

[13] S. O'Brien, A. Amann, R. Fehse, S. Osborne, E. P. O'Reilly, and J. M. Rondinelli, J. Opt. Soc. Am. B **23**, 1046 (2006).

[14] M. Sargent, M. Scully, and W. Lamb, *Laser Physics* (Addison-Wesley, Reading, Massachusetts, 1974).

[15] J. B. Khurgin, Phys. Rev. A **62**, 013821 (2000).

[16] Y. R. Shen, *The Principles of Nonlinear Optics* (Wiley, New York, 1984).

[17] I. Park, I. Fischer, and W. Elsäßer, Appl. Phys. Lett. **84**, 5189 (2004).

[18] S. Hoffmann, M. Hoffmann, E. Brundermann, M. Havenith, M. Matus, J. V. Moloney, A. S. Moskalenko, M. Kira, S. W. Koch, S. Saito, and K. Sakai, Appl. Phys. Lett. **84**, 3585 (2004).

[19] N. Owschimikow, C. Gmachl, A. Belyanin, V. Kocharovsky, D. L. Sivco, R. Colombelli, F. Capasso, and A. Y. Cho, Phys. Rev. Lett. **90**, 043902 (2003).

[20] A. Belyanin, V. Kocharovsky, V. Kocharovsky, and M. Scully, Phys. Rev. A **65**, 053824 (2002).

[21] G. P. Agrawal, Phys. Rev. A **37**, 2488 (1988).

[22] F. T. Hioe and S. Singh, Phys. Rev. A **24**, 2050 (1981).